Moisture sources for precipitation variability over the Arabian Peninsula

Matthew F. Horan[1,2] · Fulden Batibeniz[3] · Fred Kucharski[4] · Mansour Almazroui[5,6] · Muhammad Adnan Abid[4] · Joshua S. Fu[1,2,7] · Moetasim Ashfaq[1,2]

Abstract

We apply the Lagrangian-based moisture back trajectory method to two reanalysis datasets to determine the moisture sources for wet season precipitation over the Arabian Peninsula, defined as land on the Asian continent to the south of the Turkish border and west of Iran. To accomplish this, we make use of the evaporative source region between 65°W–120°E and 30°S–60°N, which is divided into twelve sub-regions. Our comparison of reanalyses and multiple observations allows us to validate datasets and highlight broad-scale similarities in characteristics, notwithstanding some inconsistencies in the southwest AP. The results indicate north-to-south spatiotemporal heterogeneity in the characteristics of dominant moisture sources. In the north, moisture for precipitation is mainly sourced from midlatitude land and water bodies, such as the Mediterranean and Caspian Seas. Areas further south are dependent on moisture transport from the Western Indian Ocean and parts of the African continent. The El Niño-Southern Oscillation (ENSO) exhibits an overall positive but sub-seasonally varying influence on the precipitation variability over the region, with noticeable moisture anomalies from all major source regions. A significant drying trend exists over parts of the Peninsula, which both reanalyses partially attribute to anomalies in the moisture advection from the Congo Basin and South Atlantic Ocean. However, considerable uncertainty in evaporation trends over the terrestrial evaporative sources in observations warrants additional modeling studies to further our understanding of key processes contributing to the negative trends.

Keywords Moisture sources · Arabian Peninsula · ENSO · Precipitation variability

✉ Matthew F. Horan
mhoran@vols.utk.edu

1 Computational Sciences and Engineering Division, Oak Ridge National Laboratory, Oak Ridge, TN, USA

2 Bredesen Center, University of Tennessee, Knoxville, TN, USA

3 Institute for Atmospheric and Climate Science, Department of Environmental Systems Science, ETH Zurich, Zurich, Switzerland

4 Section of Earth System Physics, Abdus Salam International Centre for Theoretical Physics, Trieste, Italy

5 Department of Meteorology, King Abdulaziz University, Jeddah, Saudi Arabia

6 Climatic Research Unit, School of Environmental Sciences, University of East Anglia, Norwich NR4 7TJ, UK

7 Department of Civil and Environmental Engineering, University of Tennessee, Knoxville, TN, USA

1 Introduction

The Arabian Peninsula (AP) exhibits arid climate characteristics (Abdullah and Almazroui 1998; Almazroui 2011; Almazroui et al. 2012; Edgell 2006) with limited freshwater resources, a fragile ecosystem, and fossil fuels-driven economies. More than 75% of the annual precipitation over the region is received between November and April (Abdullah and Almazroui 1998; Almazroui 2011; Almazroui et al. 2012), which is also known as the wet season. Recent decades have witnessed statistically significant warming and reduced precipitation trends across the AP (Almazroui et al. 2012), precursors of water cycle intensification. These changes in the regional climate characteristics are causing an increase in desertification that can potentially affect biodiversity and socioeconomic stability in the region. While the anthropogenic footprint is the likely cause of recent trends in the regional hydrological cycle, slow varying climate forcing, such as sea surface temperatures, is also known to influence the precipitation variability over the region. Generally, a wetter (drier) than the typical rainy season is experienced over AP during the El Niño or positive (La Niña or negative) phase of the El Niño-Southern Oscillation (ENSO) (Abid et al. 2016; Atif et al. 2020). The influence of equatorial Pacific sea surface temperature anomalies also extends to extreme precipitation events and droughts over the region. (Kang et al. 2015; Abid et al. 2018). Additionally, previous studies indicate a moderate and statistically insignificant influence of the North Atlantic Oscillation (NAO), where the region may experience a drier (wetter) than usual rainy season over northern and western portions of the AP during the positive (negative) phase of the NAO (Atif et al. 2020; Donat et al. 2014; Ehsan et al. 2017; Saeed and Almazroui 2019).

Even though a general understanding of the climate characteristics of the AP exists, there remain several gaps in our knowledge of factors impacting wet season precipitation variability. For instance, it is relatively unknown which terrestrial and oceanic evaporative sources provide moisture to the region during the wet season. Few studies suggest that much of the rainfall over the northern AP can be attributed to extratropical cyclones from the Mediterranean (Almazroui et al. 2016). However, explicit identification of moisture sources for the wet season precipitation over the AP is yet to be established. Similarly, thermodynamic pathways through which natural modes of climate variability, such as ENSO, influence precipitation distribution over the AP have not been clearly understood. Likewise, a limited mechanistic understanding of the thermodynamic factors influencing prevailing precipitation trends exists. Therefore, this study aims to improve our knowledge of AP climate by addressing knowledge gaps in the above three aspects.

Three physical sources, including moisture already present in the atmospheric column, moisture advected into the region, and moisture sourced through local evapotranspiration, facilitate precipitation over an area (Batibeniz et al. 2020; Brubaker et al. 1993; Burde and Zangvil 2001; Ciric et al. 2018; Dominguez et al. 2006; Dominguez and Kumar 2008; Drumond et al. 2011; Eltahir and Bras 1996; Gómez-Hernández et al. 2013; Schicker et al. 2010; Trenberth 1999). Most commonly, the moisture flow over or from a region is either studied by observing the spatiotemporal trajectories of moist air parcels, also known as the Lagrangian approach, or by following the moisture in-and outfluxes at fixed positions, also known as the Eulerian approach. The Lagrangian-based moisture back trajectory analysis is the most used approach due to its relatively better accuracy in determining moisture sources and sinks (Gimeno et al. 2012, 2020; Nieto et al. 2006; Sodemann et al. 2008). Other forward trajectory Lagrangian algorithms can also be effective in finding moisture sources and sinks that follow the tracks of moisture particles from evaporation to precipitation (Peng et al. 2020, 2022; Zhang et al. 2021; Stohl et al. 2005). We chose to use a back trajectory Lagrangian algorithm, Dynamic Recycling Model (DRM), developed by Dominguez et al. (2006), that we have previously applied over several regions for moisture source analyses (Ashfaq et al. 2017; Batibeniz et al. 2020; Mei et al. 2015). The details of data and moisture tracking analyses is provided in Sect. 2. Section 3 describes the main results and discussion of this analysis. Section 4 summarizes key findings and proposes future research directions. Overall, this study identifies primary evaporative sources during the wet season over the AP, describes their spatiotemporal distribution at varying scales, and explains their role in the precipitation variability during the wet season, particularly during active phases of ENSO and NAO.

2 Data and methods

2.1 Data

We use two reanalysis datasets, the Modern-Era Retrospective Analysis for Research and Application Version 2 (MERRA-2, Gelaro et al. 2017), available at 0.5° x 0.625° horizontal grid spacing, and the European Reanalysis version 5 (ERA5; Herschbach et al. 2020), available at 0.25° x 0.25° horizontal grid spacing. Multiple datasets ensure a robust understanding of moisture sources over the study region. The ERA5 dataset is remapped to the MERRA-2 horizontal grid before its use. From these datasets, we obtained four variables: daily evapotranspiration, daily precipitation, six-hourly vertically integrated eastward moisture flux, and

six-hourly vertically integrated northward moisture flux. Additionally, 850 mb monthly meridional and zonal winds are used to investigate dynamical patterns associated with global ESNO and NAO teleconnections.

Given that reanalyzed and observed precipitation is often not in high correspondence at the daily timescale, we use reanalyzed precipitation in our analyses to be consistent with the reanalyzed moisture fluxes and evapotranspiration used in the determination of moisture pathways. While this methodological choice is necessary for accuracy in calculating moisture trajectories, it may lead to inaccuracies in identifying moisture sources if the spatial distribution of precipitation substantially varies between reanalyzed and observed. Therefore, precipitation from the two reanalyses is compared with several gridded observations to understand the degree of uncertainty associated with our methodological choice. The observations include data from the University of East Anglia Climatic Research Unit (CRU; Harris et al. 2013), NOAA's Precipitation Estimation from Remotely Sensed Information using Artificial Neural Networks (PERSIANN; Sorooshian et al. 2014; Ashouri et al. 2015), the Global Precipitation Climatology Centre monthly

precipitation dataset (GPCC; Schneider et al. 2015), and the Climate Hazards Group InfraRed Precipitation with Station dataset (Funk et al. 2015). All observational datasets are also remapped to match the MERRA-2 grid spacing. Not all observations fully span our analyses period covering 1980 to 2019, as PERSIANN (GPCC) is unavailable for 1980–1982 (2017–2019).

2.2 Moisture back-trajectory analyses

We make use of the evaporative source region between 65°W–120°E along the longitudes and 30°S–60°N along the latitudes for moisture back trajectory analyses over the AP. The source region is divided into 12 sub-regions, as depicted in Fig. 1. The sub-division broadly separates known oceanic basins and large water bodies to ensure relatively accurate attribution of precipitation over the study region to remote sources. The adjacent upstream subdivisions of terrestrial areas, such as Europe, Northern Africa, and Eastern Africa, are based on the homogeneity of precipitation seasonality within a sub-region from November to April. The breakdown of the Mediterranean regions is
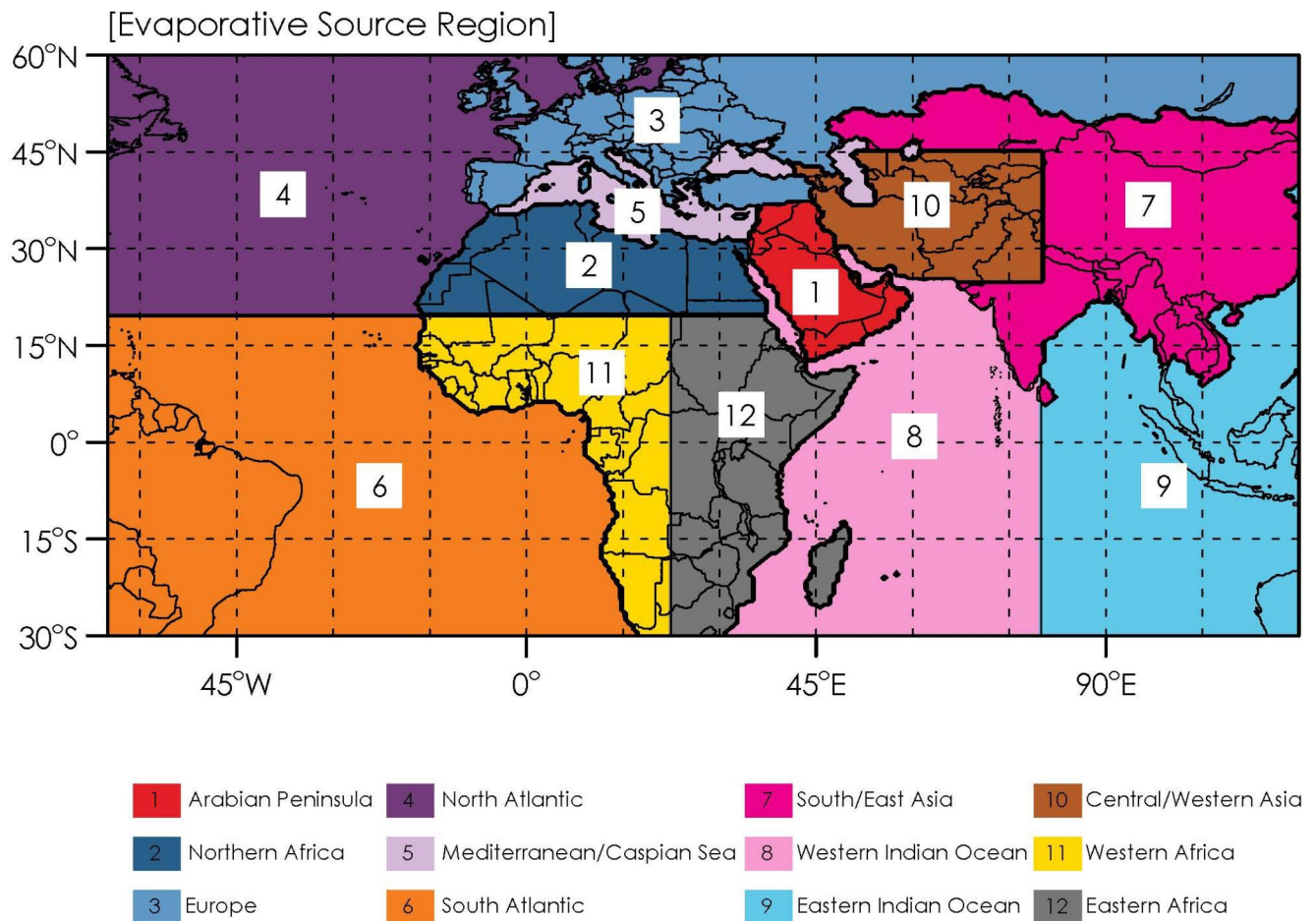

Fig. 1 Evaporative source region and its sub-divisions. Region 1 represents the study area

similar to Zittis (2018). In the more distant and downstream areas, particularly the East Asian land region and the portions of the Americas in the Atlantic Ocean regions, these considerations were curtailed as there was little contribution expected due to either distance from the target region or a downstream location. Therefore, these distant or downstream regions are broadly combined without any consideration of climate homogeneity. The twelve sub-regions (Fig. 1) include the AP as the target region (1; Asian Continent west of Iran and south of Turkey), Northern Africa (2; African continent north of 20°N), Europe land (3; all European countries including portions of Turkey and Russia in Asia), North Atlantic Ocean (4; areas west of Europe/ Africa North of 20°N), the Mediterranean and Caspian Seas (5; all water bodies between 5°W to 65°E and 29°N to 50°N), South Atlantic Ocean (6; Atlantic ocean west of African continent and south of 20°N), East Asian land (7; Asian land outside Russia and Turkey that is not in regions 1 or 10), Western Indian Ocean (8; the Indian Ocean between 30°E to 80°E and south of 31°N), Eastern Indian Ocean (9, the Indian Ocean east of 80°E), Western and Central Asia land (10; Asian continent between 40°E to 80°E and 25°N to 45°N not part of regions 1 or 3), Western Africa land (11; African continent south of 20°N and west of 22.5°E), and Eastern Africa land (12; African continent south of 20°N and east of 22.5°E). Note that the study region defined in our analyses as the AP includes northern parts of Iraq and Syria that are formally not considered a part of the Arabian Peninsula.

In the past 15 years, numerous studies across the globe have used the DRM moisture-back trajectory approach (Bisselink and Dolman 2008; Dominguez et al. 2008; Hua et al. 2017; Herrera-Estrada and Diffenbaugh 2020; Rapolaki et al. 2020). We have also applied the moisture back trajectory methodology to several other regions, including the Mediterranean by Batibeniz et al. (2020), South Asia by Ashfaq et al. (2017) and Mei et al. (2015), and Central Southwest Asia by Mehmood et al. (2022). This model was initially developed by Dominguez et al. (2006), which was modified not to include the reliance on parameterization (Dominguez et al. 2006; Gimeno et al. 2012; Stohl and James 2005). As Mei et al. (2015) described, this method applies the law of conservation of mass to water vapor while assuming a well-mixed atmosphere. Therefore, the ratio between evaporation and locally advected water vapor in the atmospheric column equals the locally recycled water to neighborly advected precipitation as determined by moisture flux data. Using a Lagrangian coordinate system, as described in Dominguez et al. (2006), the recycling ratio or amount of precipitation falling from the entire evaporative source region is defined as follows:

$$R(\chi, \xi, \tau) = 1 - \exp\left[-\int_0^\tau \frac{\epsilon(\chi, \xi, \tau)}{\omega(\chi, \xi, \tau)} d\tau\right] \quad (1)$$

(Dominguez et al. 2006) where R, ε, and ω represent the recycling ratio, evaporation, and precipitable water and χ, ξ, and τ represent the west-east, north-south, and time dimensions respectively. The time-integration term in R goes from the beginning of the calculated timeframe to the time of precipitation. The generalized equation for all regions is, therefore:

$$R(\chi, \xi, \tau 1, j)|(\tau 1 - d\tau) = R(\chi, \xi, \tau, j)|(\tau 1) - exp\left[-\int_{\tau 1 - d\tau}^\tau \frac{\epsilon(\chi, \xi, \tau)}{\omega(\chi, \xi, \tau)} d\tau\right] + exp\left[-\int_{\tau 1}^\tau \frac{\epsilon(\chi, \xi, \tau)}{\omega(\chi, \xi, \tau)} d\tau\right] \quad (2)$$

(Dominguez et al. 2006) Where $|R(\chi, \xi, \tau, j)|(\tau 1)$ shows the percentage of precipitation at a grid point (χ, ξ) contributed from grid point j at time $\tau 1$ and $d\tau$ represents the change in time. This allows us to determine the contribution from any grid point in the evaporative source region. Note that the assumption of a well-mixed atmosphere enables vertically integrated moisture flux, which may be an issue over regions with strong vertical wind shear. However, this assumption should not be a concern in this study, as the atmosphere above the AP does not exhibit a strong shear during the wet season. Also, note that data assimilation in reanalysis may violate the moisture conservation assumption; however, Dominguez et al. (2006) note that any correction for this assumption not being followed has little impact on the results. We implement our analysis from 15 October through 30 April continuously. Earlier studies have shown that water vapor resides in the atmosphere for 10 days on average (Numaguti 1999; Nieto and Gimeno 2019; Läderach and Sodemann 2016). Therefore, to ensure accuracy in the identification of moisture sources, the first 15-days are discarded to account for the residence time of moisture vapor in the atmosphere. Our study spans 39 seasons, starting with the wet season from 1 to 1980 to 30 April 1981 and ending with the wet season from 1 to 2018 to 30 April 2019.

2.3 ENSO and NAO influences

We investigate precipitation variability caused by ENSO and NAO in terms of associated moisture anomalies from source regions. ENSO is defined by the standardized Niño 3.4 index, which is the area-averaged detrended sea surface temperature anomaly over the central-eastern equatorial Pacific region (5°S to 5°N, 170°W to 120°W). NAO is defined as the standardized principal component associated with the first EOF of the detrended sea level pressure over the North Atlantic region (20°N to 80°N, 90°W to 40°E). To understand the dynamic and thermodynamic pathways taken by ENSO and NAO in establishing their teleconnection with AP precipitation, the individual and aggregated

anomalies of contributed moisture (in mm) from evaporative source regions to the AP and 850 mb winds anomalies over the entire evaporative source region are separately linearly regressed onto the standardized indices of ENSO and NAO. The regressions are performed at seasonal and two-month mean scales to investigate overall teleconnections characteristics and their sub-seasonal persistence. For these calculations, monthly atmospheric winds, sea surface temperature, sea level pressure, and precipitation are taken from the corresponding reanalyses datasets (ERA5 and MERRA2) used for moisture back trajectory calculations.

Fig. 2 Mean wet season precipitation (mm) during 1980–2019 in (**a**) CRU, (**b**) PERSIANN, (**c**) GPCC, (**d**) CHIRPS gridded observations and (**e**) MERRA2, (**f**) ERA5 reanalysis. Note that PERSIANN data was unavailable for 2017 through 2019 and GPCC data was unavailable for 1980 through 1982

3 Results and discussion

3.1 Reanalyzed versus observed precipitation and evaporation

We first examine the comparability of the precipitation distribution over the AP between the reanalyses and the observations based on the wet season (Fig. 2). Relatively high precipitation magnitudes can be observed along the Zagros Mountains in the north and the Asir and Sarat mountains in the southwest. In all datasets, the relative maximum in precipitation occurs in these regions; however, it is lessened in the GPCC and CHIRPS datasets (Fig. 2c and d,). All precipitation maxima are relatively stronger in ERA5, while CRU and PERSIANN tend to be wetter over Yemen and Oman. The precipitation distribution over central Saudi Arabia is comparable across all datasets, with CRU the driest among all. Overall, there are no distinct or systematic differences between reanalyzed and observed precipitation datasets. We further compare the percentage of annual precipitation that falls during the wet season across datasets (Fig. S1). The purpose of this comparison is twofold. First, we would like to ensure that there are no noticeable systematic differences in the intra-annual distribution of precipitation between the reanalyzed and observed datasets. Second, we want to highlight that November to April season, used in this study, covers most of the annual precipitation that falls over the region, consistent with earlier findings (Abdullah and Almazroui 1998; Almazroui 2011; Almazroui et al. 2012). Both observational and reanalyzed datasets show that over 75%, and in most cases, over 90% of the precipitation is received during the wet season used in this study. The Red Sea Coast and Asir mountains receive considerable rainfall through warm-season convection (Almazroui 2011), reflected in relatively lower (30–60%) fractions during the rainy season. There is a discrepancy among the datasets about the wet season contribution over parts of Yemen and Oman. However, this location is in the Empty Quarter, where seasonal precipitation is very low, and minor differences can lead to more considerable fractional changes. There is sub-seasonal variability in precipitation distribution which is generally comparable across datasets (Fig. S2). The Pearson correlations between area-averaged wet season precipitation over the AP during common years in the dataset can be found in Table 1. It is evident that PERSIANN and CHIRPS exhibit significant differences among the datasets, and overall, it is impossible to distinguish a systematic superiority of observations over reanalyses. These comparisons suggest no distinguishable systematic differences in reanalyzed and observed precipitation distributions. Therefore, this study's determined synoptic-scale moisture sources based on reanalyzed precipitation can be considered reliable.
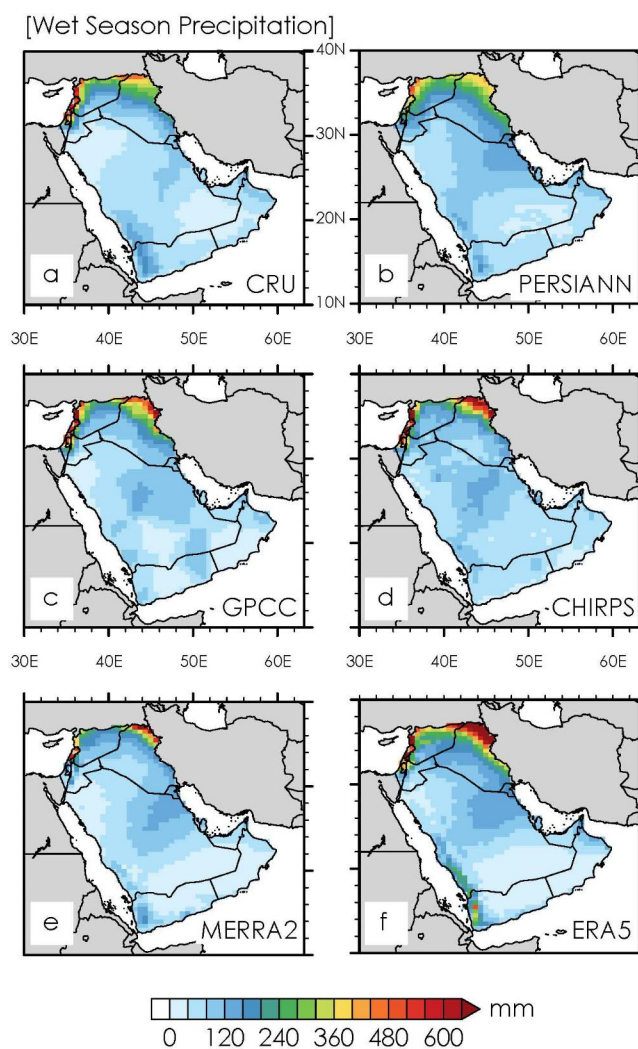
Table 1 The Pearson correlation of total area-averaged wet season precipitation in common years between datasets

	ERA5	MERRA2	CRU	PERSIANN	GPCC	CHIRPS
ERA5	1	0.95	0.90	0.66	0.97	0.77
MERRA2	0.95	1	0.82	0.68	0.92	0.65
CRU	0.90	0.82	1	0.65	0.86	0.69
PERSIANN	0.66	0.68	0.65	1	0.68	0.63
GPCC	0.97	0.92	0.86	0.68	1	0.81
CHIRPS	0.77	0.65	0.69	0.63	0.81	1

We also analyze evaporation data over the source domain during the wet season. No gridded observed evaporation data exists; therefore, analysis is limited to the evaporation from the two reanalyses (Fig. 3). The monthly evolution of evaporation (Fig. S3) shows that the mean spatial differences in evaporation throughout the wet season are much more notable than the mean temporal differences from month to month. Overall, more evaporation occurs over water bodies than inland regions, with the most vigorous land evaporation occurring near the equator.
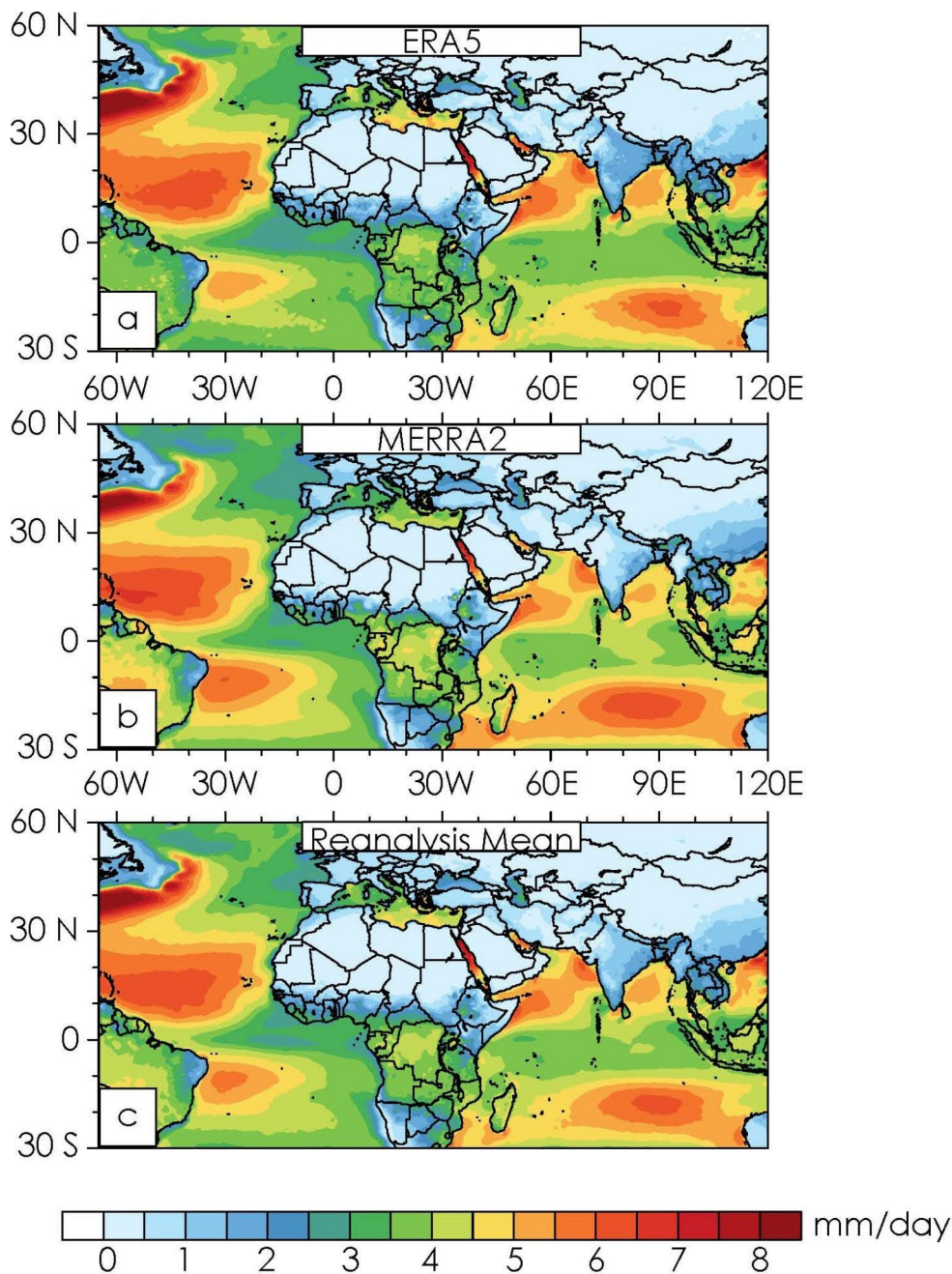
3.2 Characteristics of primary moisture sources

The fraction of moisture falling as precipitation in a grid cell that originated as evapotranspiration from the entire evaporative source region (Fig. 1), also known as the recycling ratio, is shown in Fig. 4a as an average of two datasets (ERA5 and MERRA2). The highest recycling ratio is obtained when all the precipitation is sourced back to its origin at a grid point. In this study, the recycling ratio varies between 90 and 96% (expressed in % of the total) over most of the AP, reflecting that the evaporative source domain used in this study is sufficiently large to account for the origin of almost all precipitation falling over the AP during the wet season. The contribution from the most prominent (all) source regions is shown in Fig. 4 (Fig. S4) as an average recycling ratio based on two reanalysis datasets. Panels 4e and 4f combine moderately impactful regions where moisture follows similar dynamic pathways to reach the AP. Figures S5 and S6 show individual contributions from all regions separately in ERA5 and MERRA2, respectively, while Figure S7 shows the climatological winds which provide background forcing for moisture transport in the evaporative source domain. In the north, most of the moisture comes from the Mediterranean/Caspian Seas (Fig. 4c, up to 50%), North Atlantic, and Europe (Fig. 4e, up to 40%). The primary contributors to the precipitation over this region are extratropical weather systems originating over the Mediterranean Sea and adjacent areas (Almazroui et al. 2016). These weather systems move eastward and hence have less impact on the remaining AP region in the south. Therefore, the moisture within these systems shows more influence over (up to 40%) northern Syria and Iraq, and their contribution progressively depletes southeastward. The lack of reach of extratropical weather systems over the rest of the AP diminishes contribution from the mid-latitude source regions towards the central to southern AP. In the central parts of AP, moisture advection from the African continent and South Atlantic has a sizeable contribution (Fig. 4f, up to 30% when aggregated). Potentially, a fraction of moist air near the equator over the South Atlantic and African land regions rising to the upper levels escapes towards Northern Africa and reaches the AP with the aid of the North African Jet (Figure S7).

In comparison, moisture transport from the western Indian Ocean dominates the southern half of the AP (Figs. 4b and 30 to 65%). It is important to note that the geographical footprint of moisture from the western Indian Ocean, which also includes the Arabian and Red Seas in our study, is the largest in the southern AP, with maxima over the southwestern tip of Yemen (~ 65%), and the smallest in the northern AP, with minima over the Zagros Mountains along the border of Turkey in the north (~ 5%). A relative maximum in evaporation over the Red Sea (Fig. 3) combined with the North Africa Jet allows a Red Sea trough to enhance precipitation over northern and central Saudi Arabia. At the same time, southeasterly winds advect moisture from the Arabian Sea and Gulf of Aden over the southern Arabian Peninsula. Interestingly, local moisture recycling (Figs S4-S6) does not significantly affect the precipitation distribution over the AP, as its maximum contribution remains less than ~ 10–15%. Through the western two-thirds of the target region, local recycling contribution is under 5%, indicating its less importance than advection from outside sources. The AP is overall arid, and very little moisture is available for evaporation (Fig. 3). As the ground is primarily dry, rains penetrate the soil, leaving little contact between the water and the atmosphere for evaporation. Therefore, local recycling contributes very little to atmospheric moisture over the region. Overall, the relative contribution of individual evaporative sources is comparable between ERA5 and MERRA2 (Figs. S5-S6), reflecting minor sensitivity to the choice of reanalysis to determine moisture source regions. Due to this close correspondence between the two datasets, we present the rest of the analyzed results based on their average.

Fig. 3 Mean annual evaporation (mm/day) during the entire wet season 1980–2019 in **(a)** ERA5, **(b)** MERRA2, **(c)** the mean of both reanalyses

The total recycled precipitation is the multiplicative product of the recycling ratio and the total precipitation. When the total recycled precipitation is averaged over the study region, there is considerable sub-seasonal variability in moisture contribution from individual source regions, as seen in Fig. 5, which shows the 10-day mean percent of area-averaged precipitation that can be attributed to each source region. Note that a sub-region can show high recycling ratio values over the parts of the target region (AP). However, its contribution to the area-averaged recycled precipitation over the target region may still be low if higher magnitudes of recycling ratio are over the areas that receive low seasonal precipitation magnitudes. For instance, the southern AP receives less overall precipitation; therefore, the contributions from source regions to the northern AP are more heavily weighted than the southern AP. The contribution from the Mediterranean/Caspian Seas is the highest until the beginning of March when it gradually starts diminishing. Note that the northern part of the AP, where the Mediterranean/Caspian Seas have the most significant contribution, receives relatively less rainfall towards the end of the rainy season (Fig. S2). The sub-seasonal precipitation variability over the northern AP region coincides with the annual cycle of evaporation from the Mediterranean and
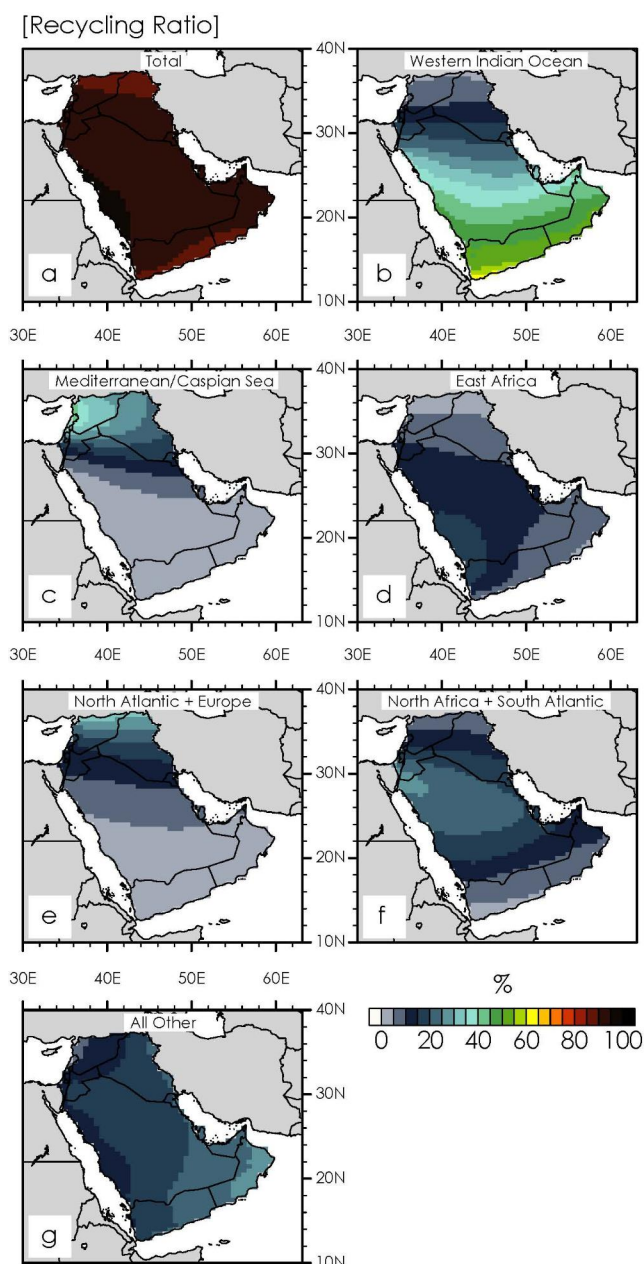
[Recycling Ratio]

[Recycled Precipitation]

Fig. 4 Average recycling ratio (expressed in % of the total) during the wet season (Nov-April). **(a)** Sum of all regions, **(b)** Western Indian Ocean, **(c)** Mediterranean and Caspian Sea, **(d)** East Africa, **(e)** sum of North Atlantic and Europe, **(f)** sum of North Africa and South Atlantic, **(g)** sum of the other regions. Results are based on the average of recycling ratio from ERA5 and MERRA2.

Fig. 5 Climatological intra-seasonal variability in regional contributions, shown as 10-day running mean area averaged over the Arabian Peninsula. Only those regions have been shown that reach a seasonal maximum of more than 5%. Note that symmetric averaging has been used at the end points. Line colors match the ones used to define regions in Fig. 1. Results are based on the average of recycling ratio from ERA5 and MERRA2.

adjacent seas that exhibits gradual decreases in the wet season with a yearly minimum in April–May (Romanou et al. 2010), explaining the decline in the moisture contribution from the Mediterranean/Caspian Sea. On the other hand, the moisture contribution from the western Indian Ocean remains relatively steady until March before strengthening to reach its maxima towards the end of the rainy season, which is consistent with relatively large amounts of rainfall

in March and April over the southern half of the AP (Fig. S2). The late-season strengthening of moisture advection from the Indian Ocean is supported by the gradual shift in the cross-equatorial flow over the ocean east of Africa (Fig. S7). The flow progressively shifts from southward in November to February to zonal in March and northwestward in April. The same dynamical changes support the subseasonal variability in the contribution from Eastern Africa, which is in sync with that from the Western Indian Ocean. Note that, over this period, the intertropical convergence zone gradually moves southward over southwest Africa (away from the AP) and back over Eastern Africa (Ashfaq et al. 2021). Some syncing is also noticed between moisture from the Mediterranean/Caspian Seas and the North Atlantic, which is understandable as similar dynamical characteristics influence the movements of storm tracks and moisture from the Mediterranean and beyond (Batibeniz et al. 2020). However, it is interesting to note that moisture contribution from Europe gradually increases over the wet season and reaches its maximum at a time when moisture supply from North Atlantic, and Mediterranean/Caspian Seas depletes.

Such an increase in moisture from a mid-latitude terrestrial source region is explicable given the annual cycle of surface temperatures that continue to rise during the AP wet season. Moreover, storm tracks continue to move north during the latter half of the wet season. The relative maximum in European contribution indicates that the storms that begin further north have more access to precipitation originating from evaporation over land in Europe.

[Regression (ENSO, (U,V, P)]

[Regression (ENSO, P)]

Fig. 6 **(a)** Regression of seasonal average winds (m/s per 1 standard deviation in ENSO) and accumulated total sourced precipitation (mm per 1 standard deviation in ENSO) anomalies onto the standardized ENSO index during the wet season. **(b-e)** same as in (a) but for the seasonal accumulated sourced precipitation from individual source regions. Black stippling represents statistical significance in precipitation changes at 90% confidence level. Blue stippling represents statistical significance in either U or V changes at 90% confidence level. The two reanalyses are averaged before regression

3.3 Thermodynamic pathways of ENSO/NAO influence over the AP

ENSO exhibits a positive association with precipitation variability over the AP, meaning that more rains are expected during the wet season when the warm phase of ENSO is active and vice versa (Abid et al. 2016; Atif et al. 2020). While earlier studies suggest above-normal moisture advection from the Indian Ocean during El Niño (Abid et al. 2016, 2020; De Vries et al. 2016), a more specific understanding of anomalies in moisture from oceanic and terrestrial moisture source regions is yet to be determined. Our analysis examines anomalies 850 mb wind anomalies and moisture anomalies from terrestrial and oceanic regions that drive ENSO influence over the AP region. We achieve this by regressing the anomalies of seasonal average winds, total sourced precipitation, and precipitation sourced from individual regions onto the standardized ENSO index, as shown in Fig. 6 and Supplementary Figure S8. The results indicate that the enhanced moisture influx during the positive phase of ENSO is not limited to the Indian Ocean, as nearly every source region shows an increase in moisture contribution (Fig. 6, S8). In particular, a statistically significant increase in moisture advection from the Indian Ocean and the African continent occurs. Note that Walker circulation disruption during El Niño causes anomalous convection (subsidence) in the western (eastern) Indian Ocean (Abid et al. 2020). As a result, an anomalous westward flow emerges over the Indian Ocean in the lower atmosphere, reflected in the regressed 850 mb winds map (Fig. 6a). Increased (decreased) winter moisture convergence over the western Indian Ocean during El Niño (La Niña) episode is consistent with previous research (Castillo et al. 2014). These conditions favor enhanced moisture advection from the Western and Eastern Indian Ocean and northern parts of Eastern Africa.

Moreover, wetter than normal conditions are well known over equatorial and Eastern Africa during the warm phase of ENSO (Mbigi and Xiao 2021), meaning that more moisture is available to be transported to the AP from those areas. Additionally, with weakened easterlies and more divergence in equatorial Africa during ENSO (Spinks and Lin 2014), less moisture already available near the equator is advected towards the tropical Atlantic Oceans. Thus, a more significant percentage of precipitation advected out of equatorial Africa becomes available for transportation to other regions. Excessive moisture transport is also witnessed from Europe and the Mediterranean/Caspian Seas. It is well known that the warm phase of ENSO favors the southward shift in the extratropical cyclones, causing enhanced moisture advection from the mid-latitude source regions over the northern AP. However, most of these increases are not statistically
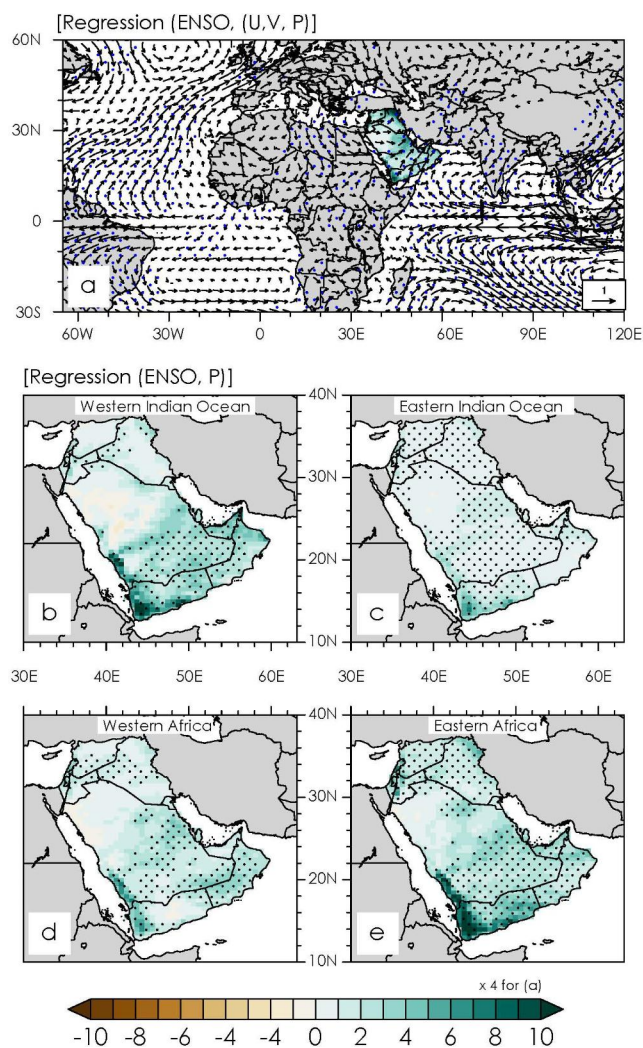
significant. Local recycling also exhibits a noticeable rise in Iraq and Saudi Arabia along the Arabian Gulf (Fig. S8).

Substantial sub-seasonal variability in ENSO teleconnection and associated moisture anomalies from respective source regions exists over the AP (Figs. S9-S11). Overall, ENSO teleconnection becomes insignificant and reverses over Iraq and adjacent Saudi Arabia region in Jan–Feb creating a reversal in moisture anomalies from primary source regions (Europe, North Atlantic, and Mediterranean/Caspian Seas). The circulation anomalies in the lower atmosphere (850 mb) exhibit anomalous dry air entrainment from northern Africa during Jan–Feb in contrast to the rest of the season, where moisture advection from the abovementioned source regions is favored (Figs. S9-S11). The insignificance of ENSO's role during Jan–Feb has also been noted in earlier studies focused on the broader Central Southwest Asia region (Abid et al. 2020; Mehmood et al. 2022). According to these studies, ENSO influences this region through

a combination of direct Rossby-wave teleconnection originating in the equatorial Pacific and indirect teleconnection resulting from interbrain interactions between the Pacific and Indian Oceans through the Walker circulation-driven atmospheric bridge. When the two teleconnection pathways of ENSO are in phase, its influence is greatest, and when they are out of phase, its influence is lowest. At the individual level, the increase in contribution from Eastern Africa and the western Indian Ocean is statistically more robust during Nov–Feb (Figs. S9-S10), coinciding with the period when ENSO forcing is typically the strongest. However, the anomalous moisture contribution from the Southern Atlantic only becomes significant between Mar and Apr (Fig. S11), coinciding with the time when this region's moisture contribution is strongest. Near the equatorial belt over east Africa, ENSO teleconnections lead to onshore wind anomalies from the Indian Ocean, and winds over land change direction in Mar–Apr, limiting the moisture advection from these regions to the AP, while an increase in precipitation from the extratropics is still reflected from the Mediterranean (Fig. S11).

As previously noted, NAO's influence on the AP climate is not as robust as it is in the case of ENSO. To investigate the characteristics of circulation and moisture anomalies shaping NAO teleconnection, we perform regression analyses identical to those presented in Fig. 6 and Supplementary Figures S8 to S11 by replacing the standardized ENSO index with the NAO index. These results are shown in Fig. 7 and Supplementary Figures S12 to S15. A positive phase of NAO causes the westerlies over the Mediterranean and northern Africa to weaken, decreasing the amount of moisture that advects from Europe and the northern Atlantic into the target region (Fig S12). Spatially, the moisture change from the NAO teleconnection exhibits a dipolar pattern over the AP, with a negative association in the northern two-thirds and a positive association in the southern one-third. However, this negative influence over that region is mostly statistically insignificant (Fig. 7a) due to a lack of robustness in moisture anomalies from the primary source regions (Fig. 7b and d). More specifically, the negative association in the northern two-thirds is caused by reduced moisture advection from Europe and the northern Atlantic and potentially a westward movement in Mediterranean storm tracks. While the moisture advection from the Mediterranean/Caspian Seas also decreases significantly over parts of central Saudi Arabia, its reduction is insignificant over Syria. In contrast, it shows a mixed response over Iraq. The positive association over the parts of southern AP is due to an enhanced moist advection from Western African, Indian Ocean, and Eastern Africa, and more local recycling (Fig. S12), consistent with an increase in precipitation near the Arabian Sea shown in previous research (Nieto et al. 2014).
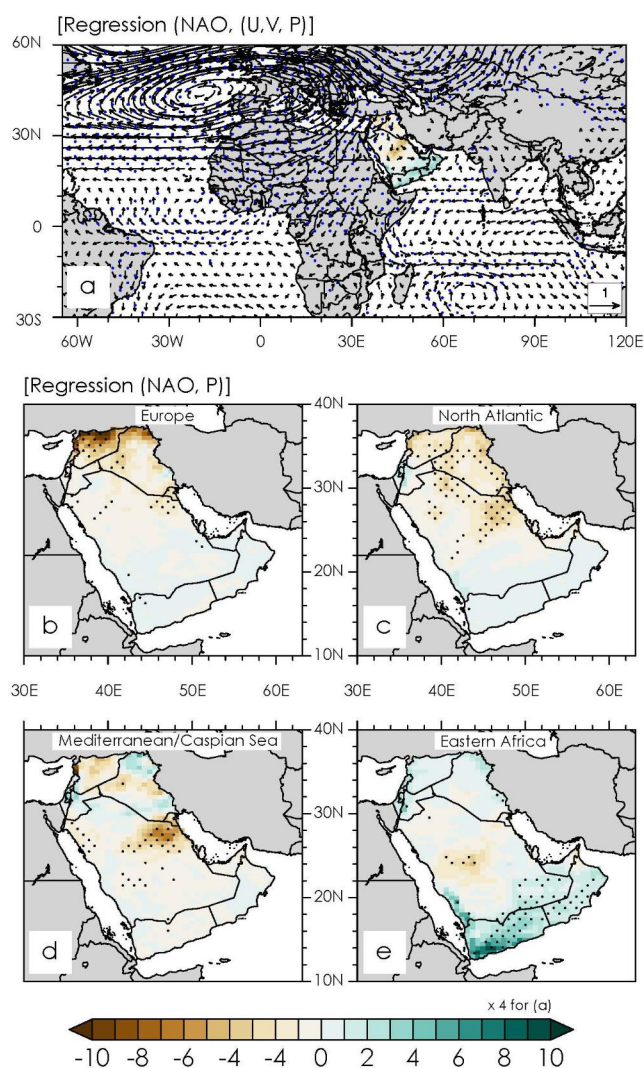

Fig. 7 Same as in Fig. 6 but for NAO.

The effects of NAO teleconnection over the AP also exhibits sub-seasonal variability (Figs. S13-S15). For instance, the statistically significant negative NAO association over the central AP only exists during Nov–Dec, when moisture supply from most prominent sources decreases. Due to below normal moisture transport from major moisture sources in Nov–Dec, local recycling also becomes significantly limited over eastern Saudi Arabia and Kuwait (Fig S13). Similarly, an increase in moisture advection from the Indian Ocean and parts of Africa over the southern AP is only significant during Mar–Apr. In general, as the wet season progresses, precipitation associated with the NAO changes direction and generally decreases in magnitude as the rainy season progresses (Figs. S13-15). This potentially implies that the NAO impact lessens over the course of the wet season. The lack of sub-seasonal persistence in NAO teleconnection is consistent with variations in ENSO influence over the AP.

Overall, there is substantial variation in sub-seasonal moisture advection anomalies caused by remote forcings, such as ENSO and NAO, during the wet season. Perhaps, it is this sub-seasonal inconsistency in moisture advection from evaporative sources that is the cause of the lack of persistence in the ENSO and NAO teleconnections during the wet season, which may result in the limited precipitation prediction skill over the region (Abid et al. 2016; Ehsan et al. 2017).

3.4 Wet season precipitation trends

We use the Mann-Kendall test to calculate trends in total precipitation and moisture contribution from respective evaporative sources and test their significance at a 95% confidence level. The trends in moisture contribution from each source are shown in Fig. 8, while wet season precipitation trends over the AP and the entire source region are shown in supplementary Figures S16 and S17 respectively. Generally, the wet season precipitation over the AP exhibits negative trends (Fig. S16). Unfortunately, the spatial trends are inconsistent across observational datasets and between observations and reanalyses over much of the AP. The lack of correspondence among observational datasets is likely due to an insufficient number of ground observations over the region (Zittis 2018) and differences in grid mapping techniques. Some gridded observations rely on ground observations, while others blend remotely sensed data with ground observations. Nonetheless, more research is needed to understand the sources of uncertainty in gridded observations and their connection with the precipitation trends over the AP.

Although there are disagreements among datasets, the negative precipitation trends over the central and southwestern AP region are relatively robust across observations and reanalyses. Recent studies based on station observations have consistently demonstrated that the central AP is witnessing a decrease in precipitation, leading to more severe droughts (Alsaarann and Alghmadi 2021; Syed et al. 2022). Therefore, we limit our focus to this area, where we assume the drying trend is robust, to understand the potential causes of these trends. Considering that moisture source analyses are based on the reanalyzed data, the trends in moisture advection from individual moisture sources, shown in Fig. 8, should provide insight into precipitation trends in the reanalyzed precipitation over the AP. The analysis of trends in moisture contribution from source regions suggests that negative precipitation trends over the central and southwestern AP (Fig. S16) are driven mainly by reduced moisture advection from Western Africa, the South Atlantic, Western Indian Ocean, and Eastern Africa (in order of significant). When trends of both precipitation and evaporation are analyzed over the terrestrial parts of the evaporative source region, both ERA5 and MERRA2 display statistically significant strong negative trends over the Congo basin and parts of central Africa (Figs. S17, evaporation in S18) – the area which is partitioned as Western Africa in our subdivision of moisture sources (Fig. 1). This region experiences a dry season between Nov to March (Ashfaq et al. 2021), which is why moisture contribution from Western Africa gradually increases during the wet season over the AP (Fig. 5; mustard line). Studies have shown that dry season length has recently increased over Equatorial Africa (Froidurot and Diedhiou 2017), leading to less overall moisture available for evaporation. With less terrestrial evaporation, the northward moisture fluxes from equatorial Africa should reduce. Indeed, reanalyses-based evaporation trends (Fig. S18) show a decrease in these areas, supporting evidence that these may be related to reduced precipitation in equatorial Africa. However, it is essential to note that these patterns are not seen in all observational datasets, so there is still significant uncertainty in this finding (Figs. S16-S17). As previously mentioned, the moisture contribution from the Eastern African region also exhibits a decline over the southwestern AP, which is present in both reanalyses (Figs. S19-S20). This reduction in moisture supply from Eastern Africa is most likely due to a drying trend over the Ethiopian highlands, which is present in both datasets, leading to an overall decrease in precipitation in the circulations over central Africa. Most gridded observations also show a negative trend over the Ethiopian highlands (Fig. S17). Despite the noticeable differences between the reanalysis and observations in the spatial distribution of precipitation trends over the evaporative source region, the dependence of AP precipitation on the terrestrial evaporative sources demonstrates how precipitation trends over one source region can impact

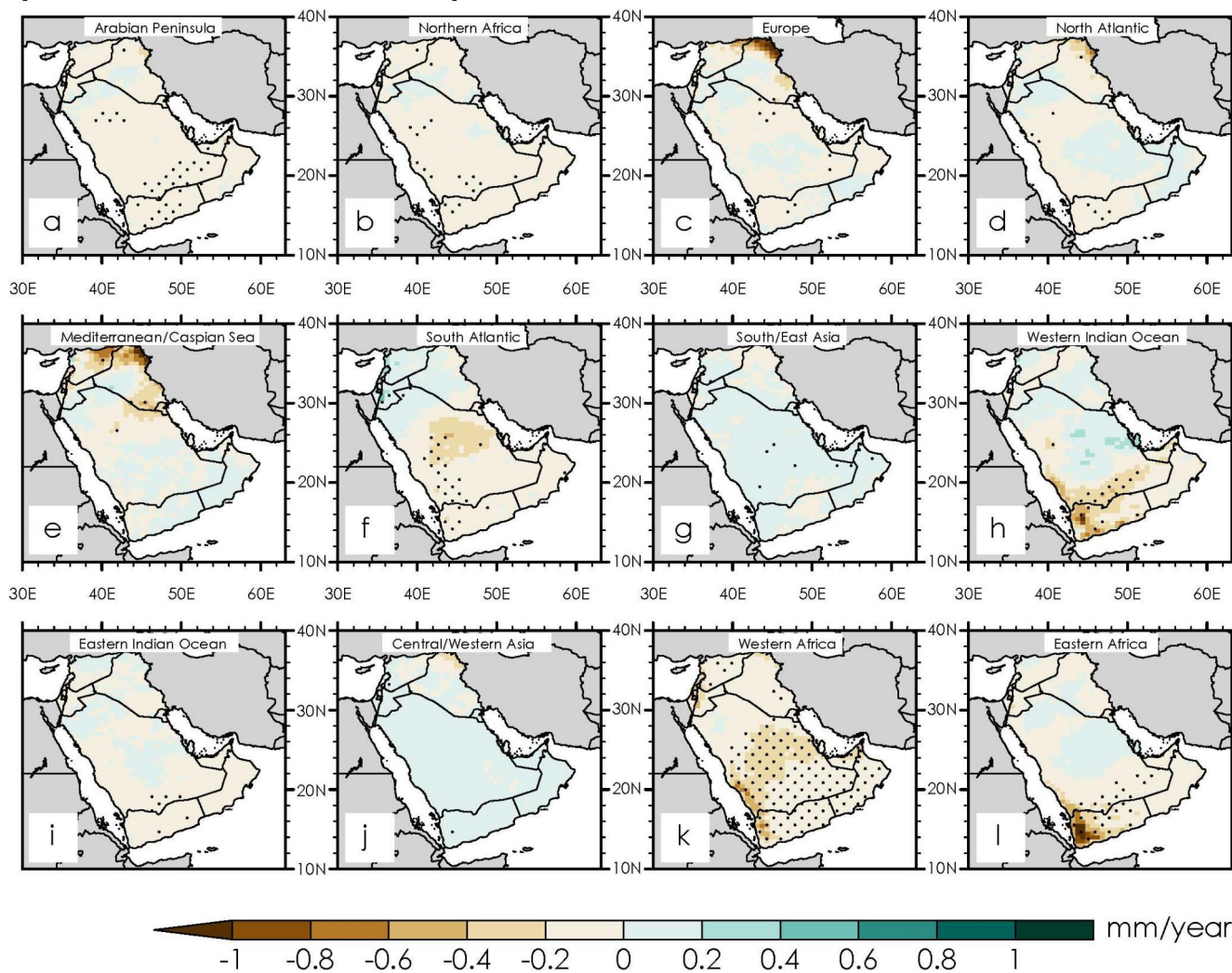## [Trends in Seasonal Contribution]

Fig. 8 Trends (mm/year) in seasonal accumulated contribution from each source region over 1980–2019. Stippling indicates significance at 95% confidence level. Trends are based on the average of ERA5 and MERRA2.

precipitation distribution over a distant sink region and highlight the complexity and intricacy of thermodynamic drivers influencing the precipitation variability over an area. Although we are seeing an increase in evaporation over the ocean sources (Fig S18), this does not translate to advection into the AP, indicating further that much of the variability in the AP precipitation with a warming atmosphere is due to the changes in evaporation over terrestrial sources. Overall, these findings suggest that changes in evaporation over a warming ocean are less impactful in determining prevailing AP precipitation trends than the changes in evaporation over terrestrial source regions.

Considering that precipitation trends over the AP and central/western Africa are accurate in the two reanalyses, it implies that the processes that govern the variability of AP climate are complex. It is important to note that moisture transport from the tropical South Atlantic is a major factor in influencing the Congo basin and adjacent areas (Sorí et al. 2017). Both regions exhibit a negative trend in moisture contribution to the AP. As a result, it is not unreasonable to assume that the South Atlantic has a significant influence on precipitation trends in the southwest and central latitudes of the AP, both directly and indirectly (via the Congo basin) influences on the AP climate. We should note that the combined maximum moisture contribution from these regions (Western Africa and South Atlantic) over any part of the AP does not exceed 15–20% of the total. However, a substantial reduction in moisture contribution from these areas can still have a significant impact the AP climate.

4 Summary and conclusions

Arid regions, such as the AP, receive moisture primarily through advection from other sources. Except for the northern regions of the AP, where extratropical storms transport moisture from mid-latitude evaporative sources, the rest of the AP receives most of its moisture from the Western Indian Ocean and some from the African continent. There is the greatest spatial variability in moisture contribution from the Western Indian Ocean, which shows a gradient from west-southwest to north (Fig. 4, S4-S6). A sub-seasonal variation in moisture sources drives a spatial variation in precipitation distribution over the AP during the wet season. The anomalies in moisture advection from source regions also vary sub-seasonally in response to remote forcings, such as ENSO and NAO, which contributes to a lack of persistence in their teleconnection. A robust drying trend over the AP in recent years has also been noted. It is possible that this drying is related to similar thermodynamic trends over equatorial Africa, but further analysis and modeling studies are required in order to establish these connections with confidence.

Overall, this study advances our knowledge of the thermodynamic processes leading to wet season precipitation over the AP. More specifically, it provides new insights into the thermodynamic structure of the AP's climate, its sub-seasonal and interannual variability, and the pathways taken by important modes of climate variability (ENSO, NAO) impacting this region. A significant fraction of moisture over the AP is transported from the terrestrial source regions (African and European continents), so climate variability on different timescales in those regions can affect precipitation distribution over the AP. Even so, there are still several gaps in our understanding of such interdependencies of terrestrial climates, which warrant further studies. The inconsistency in trends between multiple observational datasets, which is more consistent between reanalysis than among observations, leaves some uncertainties in our conclusions and should inspire further research to test whether the thermodynamic pathways identified in our analyses are valid through numerical model experiments. It is important to note that we only looked at direct pathways by which ENSO and NAO influence AP precipitation variability. In reality, teleconnections among natural modes of variability, such as ENSO, often result from multiple pathways, such as inter-basin interactions (Abid et al. 2020), and tropical-extratropical interactions (Mehmood et al. 2022). The physical mechanisms responsible for these teleconnections should therefore be investigated in more depth. Despite these caveats, this study has enhanced knowledge of precipitation variability in the region and its thermodynamic processes.

Declarations

References

Abdullah MA, Al-Mazroui M (1998) Climatological study of the southwestern region of Saudi Arabia. I. Rainfall Analysis. Clim Res 9:213–223. https://www.jstor.org/stable/24864531

Abid MA, Kucharski F, Almazroui M, Kang IS (2016) Interannual rainfall variability and ECMWF-Sys4-based predictability over the Arabian Peninsula winter monsoon region. Q J R Meteorol Soc 142:233–242. https://doi.org/10.1002/qj.2648

Abid MA, Almazroui M, Kucharski F, O'Brien E, Yousef AE (2018) ENSO relationship to summer rainfall variability and its potential

predictability over Arabian Peninsula region. Npj Clim Atmospheric Sci 1(1). https://doi.org/10.1038/s41612-017-0007-3

Abid MA, Ashfaq M, Kucharski F, Evans KJ, Almazroui M (2020) Tropical Indian Ocean mediates ENSO influence over Central Southwest Asia during the wet season. Geophys Res Lett 47:e2020GL089308. https://doi.org/10.1029/2020GL089308

Almazroui M (2011) Calibration of TRMM rainfall climatology over Saudi Arabia during 1998–2009. Atmos Res 99:400–414. https://doi.org/10.1016/j.atmosres.2010.11.006

Almazroui M, Islam MN, Athar H, Jones PD, Rahman MA (2012) Recent climate change in the Arabian Peninsula: annual rainfall and temperature analysis of Saudi Arabia for 1978–2009. Int J Climatol 32:953–966. https://doi.org/10.1002/joc.3446

Almazroui M, Kamil S, Ammar K, Keay K, Alamoudi AO (2016) Climatology of the 500-hPa mediterranean storms associated with Saudi Arabia wet season precipitation. Clim Dyn 47:3029–3042. https://doi.org/10.1007/s00382-016-3011-0

Alsaaran N, Alghmadi AS (2021) Precipitation climatology and spatiotemporal trends over the Arabian Peninsula. Theor Appl Climatol 147:1133–1149. https://doi.org/10.1007/s00704-021-03878-5

Ashfaq M, Cavazos T, Reboita MS, Torres-Alavez JA, Im ES, Olusegun CF, Alves L, Key K, Adeniyi MO, Tall M, Sylla MB, Mehmood S, Zafar Q, Das S, Diallo I, Coppola E, Giorgi F (2021) Robust late twenty-first century shift in the regional monsoons in RegCM-CORDEX simulations. Clim Dyn 57:1463–1488. https://doi.org/10.1007/s00382-020-05306-2

Ashfaq M, Rastogi D, Mei R, Touma D, Leung R (2017) Sources of errors in the simulation of south asian monsoon in CMIP5 GCMs. Clim Dyn 49:193–223. https://doi.org/10.1007/s00382-016-3337-7

Ashouri H, Hsu K, Sorooshian S, Braithwaite DK, Knapp KR, Cecil LD, Nelson BR, Pratt OP (2015) Bull Am Meteorol Soc 96(1):69–83. https://doi.org/10.1175/BAMS-D-13-00068.1. PERSIANN-CDR: Daily Precipitation Climate Data Record from Multisatellite Observations for Hydrological and Climate Studies

Atif RM, Almazroui M, Saeed S, Abid MA, Islam MN, Ismail M (2020) Extreme precipitation events over Saudi Arabia during the wet season and their associated teleconnections. Atmos Res 231:104655. https://doi.org/10.1016/j.atmosres.2019.104655

Batibeniz F, Ashfaq M, Önol B, Turuncoglu U, Mehmoud S, Evans K (2020) Identification of major moisture sources across the Mediterranean Basin. Clim Dyn 54:4109–4127. https://doi.org/10.1007/s00382-020-05224-3

Bisselink B, Dolman AJ (2008) Precipitation recycling: moisture sources over Europe using ERA-40 data. J Hydrometeorol 9(5):1073–1083. https://doi.org/10.1175/2008JHM962.1

Brubaker KL, Entekhabi D, Eagleson PS (1993) Estimation of continental precipitation recycling. J Clim 6:1077–1089. https://doi.org/10.1175/15200442(1993)006%3c1077. :EOCPR%3e2.0.CO;2,

Burde GI, Zangvil A (2001) The estimation of regional precipitation recycling. Part I: review of recycling models. J Clim 14:2497–2508. https://doi.org/10.1175/1520-0442(2001)014<2497:TEORPR>2.0.CO;2

Castillo R, Nieto R, Drumond A, Gimeno L (2014) The role of the ENSO cycle in the modulation of moisture transport from major oceanic moisture sources. Water Resour Res 50:1046–1058. https://doi.org/10.1002/2013WR013900

Ciric D, Nieto R, Losada L, Drumond A, Gimeno L (2018) The Mediterranean moisture contribution to Climatological and Extreme Monthly Continental Precipitation. Water 10:519. https://doi.org/10.3390/w10040519

De Vries AJ, Feldstein SB, Riemer M, Tyrlis E, Sprenger M, Baumgart M, Fnais M, Lelieveld J (2016) Dynamics of tropical–extratropical interactions and extreme precipitation events in Saudi Arabia in autumn, winter and spring. Q J R Meteorol Soc 142(697):1862–1880. https://doi.org/10.1002/qj.2781

Dominguez F, Kumar P (2008) Precipitation recycling variability and ecoclimatological stability—a study using NARR data. Part I: Central U. S. Plains Ecoregion. J Clim 21:5165–5186. https://doi.org/10.1175/2008JCLI1756.1

Dominguez F, Kumar P, Vivoni E (2008) Precipitation recycling variability and Ecoclimatological Stability—A Study using NARR Data. Part II: north american Monsoon Region. J Clim 21:5187–5203. https://doi.org/10.1175/2008JCLI1760.1

Dominguez F, Kumar P, Liang X-Z, Ting M (2006) Impact of atmospheric moisture storage on precipitation recycling. J Clim 19:1513–1530. https://doi.org/10.1175/JCLI3691.1

Donat MG, Peterson TC, King AD, Almazroui M, Kolli RK, Boucherf D, Al-Mulla AY, Nour AY, Aly AA, Nada TAA, Semawi MM, Al Dashti HA, Salhab TG, El Fadli KI, Muftah MK, Eida SD, Badi W, Driouech F, El Rhaz K, Abubbaker MJY, Al Dhanhani JS, Al Shekaili MN (2014) Changes in extreme temperature and precipitation in the arab region: long-term trends and variability related to ENSO and NAO. Int J Climatol 34:581–592. https://doi.org/10.1002/joc.3707

Drumond A, Nieto R, Hernandez E, Gimeno L (2011) A lagrangian analysis of the variation in moisture sources related to drier and wetter conditions in regions around the Mediterranean Basin. Nat Hazards Earth Syst Sci 11:2307–2320. https://doi.org/10.5194/nhess-11-2307-2011

Edgell HS (2006) Arabian deserts: nature, origin, and evolution. Springer, Berlin. https://doi.org/10.1007/1-4020-3970-0

Ehsan MA, Tippett MK, Almazroui M, Ismail M, Yousef A, Kucharski F, Omar M, Hussein M, Alkhalaf AA (2017) Skill and predictability in multimodel ensemble forecasts for Northern Hemisphere regions with dominant winter precipitation. Clim Dyn 48:3309–3324. https://doi.org/10.1007/s00382-016-3267-4

Eltahir EAB, Bras RL (1996) Precipitation recycling. Rev Geophys 34:367–378. https://doi.org/10.1029/96RG01927

Froidurot S, Diedhiou A (2017) Characteristics of wet and dry spells in the west african monsoon system. Atmos Sci Lett 18:125–131. https://doi.org/10.1002/asl.734

Funk C, Peterson P, Landsfeld M, Pedreros D, Verdin J, Shukla S, Husak G, Rowland J, Harrison L, Hoell A, Michaelsen J (2015) The climate hazards infrared precipitation with stations—a new environmental record for monitoring extremes. Sci Data 2(1). https://doi.org/10.1038/sdata.2015.66

Gelaro R, Mccarty W, Suárez RT, Molod A, Takacs L, Randles CA, Darmenov A, Bosilovich MG, Reichle R, Wargan K, Coy L, Cullather R, Draper C, Akella S, Buchard V, Conaty A, Da Silva AM, Gu W, Kim GK, Koster R, Lucchesi R, Merkova D, Nielsen JE, Partyka G, Pawson S, Putman W, Rienecker M, Schubert SD, Sienkiewicz M, Zhao B (2017) The Modern-Era Retrospective Analysis for Research and Applications, Version 2 (MERRA-2). J. Clim 30(14):5419 – 454. https://doi.org/10.1175/jcli-d-16-0758.1.1

Gimeno L, Stohl A, Trigo RM, Dominguez F, Yoshimura K, Yu L, Drumond A, Durán-Quesada AM, Nieto R (2012) Oceanic and terrestrial sources of continental precipitation. Rev Geophys 50:RG4003. https://doi.org/10.1029/2012RG000389

Gimeno L, Vázquez M, Eiras-Barca J, Sorí R, Stojanovic M, Algarra I, Nieto R, Ramos AM, Durán-Quesada AM, Dominguez F (2020) Recent progress on the sources of Continental Precipitation as revealed by moisture transport analysis. Earth-Sci Rev 103070. https://doi.org/10.1016/j.earscirev.2019.103070

Gómez-Hernández M, Drumond A, Gimeno L, Garcia-Herrera R (2013) Variability of moisture sources in the Mediterranean region during the period 1980–2000: variability of Mediterranean moisture sources. Water Resour Res 49:6781–6794. https://doi.org/10.1002/wrcr.20538

Harris I, Jones P, Osborn T, Lister D (2013) Updated high-resolution grids of monthly climatic observations - the CRU TS3.10 dataset. Int J Climatol 34(3):623–642. https://doi.org/10.1002/joc.3711

Herrera-Estrada JE, Diffenbaugh NS (2020) Landfalling droughts: global tracking of moisture deficits from the oceans onto land. Water Resour Res 56. https://doi.org/10.1029/2019WR026877. e2019WR026877

Hersbach H, Bell B, Berrisford P, Hirahara S, Horányi A, Muñoz-Sabater J, Nicolas J, Peubey C, Radu R, Schepers D, Simmons A, Soci C, Abdalla S, Abellan X, Balsamo G, Bechtold P, Biavati G, Bidlot J, Bonavita M, De Chiara G, Dahlgren P, Dee D, Diamantakis M, Dragani R, Flemming J, Forbes R, Fuentes M, Geer A, Haimberger L, Healy S, Hogan RJ, Hólm E, Janisková M, Keeley S, Laloyaux P, Lopez P, Lupu C, Radnoti G, de Rosnay P, Rozum I, Vamborg F, Villaume S, Thépaut JN (2020) The era5 global reanalysis. Q J Royal Meteorol Soc. https://doi.org/10.1002/qj.3803

Hua L, Zhong L, Ke Z (2017) Characteristics of the precipitation recycling ratio and its relationship with regional precipitation in China. Theor Appl Climatol 127:513–531. https://doi.org/10.1007/s00704-015-1645-1

Kang IS, Rashid IU, Kucharski F, Almazroui M, Abdulrahman KA (2015) Multidecadal changes in the relationship between ENSO and wet-season precipitation in the Arabian Peninsula. J Clim 28(12):4743–4752. https://doi.org/10.1175/JCLI-D-14-00388.1

Läderach A, Sodemann H (2016) A revised picture of the atmospheric moisture residence time. Geophys Res Lett 43:924–933. https://doi.org/10.1002/2015GL067449

Mbigi D, Xiao Z (2021) Tanzanian rainfall responses to El Niño and positive Indian Ocean Dipole events during 1951–2015. Atmospheric and Oceanic Science Letters 10093. https://doi.org/10.1016/j.aosl.2021.100093

Mehmood S, Ashfaq M, Kapnick S, Gosh S, Abid MA, Kucharski F, Batibeniz F, Saha A, Evans K, Hsu HH (2022) Dominant controls of cold-season precipitation variability over the high mountains of Asia. Npj Clim Atmos Sci 5(65). https://doi.org/10.1038/s41612-022-00282-2

Mei R, Ashfaq M, Rastogi D, Leung LR, Dominguez F (2015) Dominating controls for wetter south asian summer monsoon in the twenty-first century. J Clim 28:3400–3419. https://doi.org/10.1175/JCLI-D-14-00355

Nieto R, Castillo R, Drumond A (2014) The modulation of oceanic moisture transport by the hemispheric annular modes. Front Earth Sci 2. https://doi.org/10.3389/feart.2014.00011

Nieto R, Gimeno L (2019) A database of optimal integration times for Lagrangian studies of atmospheric moisture sources and sinks, Sci Data 6(59) https://doi.org/10.1038/s41597-019-0068-8

Nieto R, Gimeno L, Trigo RM (2006) A lagrangian identification of major sources of Sahel moisture. Geophys Res Lett 33:L18707. https://doi.org/10.1029/2006GL027232

Numaguti A (1999) Origin and recycling processes of precipitating water over the eurasian continent: experiments using an atmospheric general circulation model. J Geophys Res 104(D2):1957–1972. https://doi.org/10.1029/1998JD200026

Peng D, Zhou T, Zhang L (2020) Moisture sources associated with precipitation during dry and wet seasons over Central Asia. J Clim 33(24):10755–10771. https://doi.org/10.1175/JCLI-D-20-0029.1

Peng D, Zhou T, Sun Y, Lin A (2022) Interannual variation in moisture sources for the First Rainy season in South China estimated by the FLEXPART Model. J Clim 35(2):745–761. https://doi.org/10.1175/JCLI-D-21-0289.1

Rapolaki RS, Blamey RC, Hermes JC, Reason CJC (2020) Moisture sources associated with heavy rainfall over the Limpopo River Basin, southern Africa. Clim Dyn 55:1473–1487. https://doi.org/10.1007/s00382-020-05336-w

Romanou A, Tselioudis G, Zerefos CS, Clayson CA, Curry JA, Andeson A (2010) Evaporation–precipitation variability over the Mediterranean and the Black Seas from Satellite and Reanalysis Estimate. J Clim 23(19):5268–5287. https://doi.org/10.1175/2010JCLI3525.1

Saeed S, Almazroui M (2019) Impacts of mid-latitude circulation on winter precipitation over the Arabian Peninsula.Clim. Dyn.53:5253–5264 https://doi.org/10.1007/s00382-019-04862-6

Schicker I, Radanovics S, Seibert P (2010) Origin and transport of Mediterranean moisture and air. Atmos Chem Phys 10(11):5089–5105. https://doi.org/10.5194/acp-10-5089-2010

Schneider U, Becker A, Finger P, Meyer-Christoffer A, Rudolf B, Ziese M (2015) GPCC Full Data Reanalysis Version 6.0 at 0.5°: Monthly Land-Surface Precipitation from Rain-Gauges built on GTS-based and Historic Data. https://doi.org/10.5676/DWD_GPCC/FD_M_V7_050

Sodemann H, Schwierz C, Wernli H (2008) Interannual variability of Greenland winter precipitation sources: lagrangian moisture diagnostic and north Atlantic Oscillation influence. J Geophys Res 113:D03107. https://doi.org/10.1029/2007JD008503

Sorí R, Nieto R, Vicente-Serrano SM, Drumond A, Gimeno L (2017) A lagrangian perspective of the hydrological cycle in the Congo River basin. Earth Syst Dynam 8:653–675. https://doi.org/10.5194/esd-8-653-2017

Sorooshian S, Hsu K, Braithwaite D, Ashouri H, Program NOAACDR (2014) NOAA Climate Data Record (CDR) of precipitation estimation from remotely sensed information using Artificial neural networks (PERSIANN-CDR), Version 1 revision 1. https://doi.org/10.7289/V51V5BWQ. NOAA National Centers for Environmental Information

Stohl A, Forster C, Frank A, Wotawa G (2005) Technical note: the Lagrangian particle dispersion model FLEXPART version 6.2. Atmos Chem Phys 5:2461–2474. https://doi.org/10.5194/acp-5-2461-200

Stohl A, James P (2005) A lagrangian analysis of the atmospheric branch of the global water cycle. Part II: moisture transports between earth's ocean basins and river catchments. J Hydrometeorol 6:961–984. https://doi.org/10.1175/JHM470.1

Spinks J, Lin YL (2014) Variability of the Subtropical Highs, African Easterly Jet and Easterly Wave Intensities over North Africa and Arabian Peninsula in late summer. Int J Climatol 35(12):3540–3555. https://doi.org/10.1002/joc.4226

Syed FS, Adnan S, Zamreeq A, Ghulam A (2022) Identification of droughts over Saudi Arabia and global teleconnections. Nat Hazardshttps://doi.org/10.1007/s00704-021-03878-5

Trenberth KE (1999) Atmospheric moisture recycling: role of advection and local evaporation. J Clim 12:1368–1381. https://doi.org/10.1175/1520-0442(1999)012%3c1368.AMRROA%3e2.0.CO;2

Zhang S, Liu B, Ren G, Zhou T, Jiang C, Li S, Su B (2021) Moisture sources and paths associated with warm-season precipitation over the Sichuan Basin in southwestern China: climatology and interannual variability. J Hydrol 603B:127019. https://doi.org/10.1016/j.jhydrol.2021.127019

Zittis G (2018) Observed rainfall trends and precipitation uncertainty in the vicinity of the Mediterranean, Middle East and North Africa. 134:1207–1230. https://doi.org/10.1007/s00704-017-2333-0